An MMC With Integrated Energy Dissipation Function Using Thyristor-Based Chopper Modules for the Offshore Wind VSC-HVDC System

Sihang Wu, Lei Qi, Meichen Jin, Zhiguo He, and Xiangyu Zhang

***Abstract*—The dc chopper (DCC) is the key equipment to realize the ac fault ride through (FRT) of the offshore wind voltage source converter (VSC)-HVdc system. The existing DCC is arranged independently, and the full control device is used to control the absorbed surplus power, which is costly and limits its further application. In this article, an modular multilevel converter (MMC) with integrated energy dissipation function using thyristor-based chopper modules (TCM MMC) is proposed. It distributes the chopper module that dissipates the surplus power of the system into the submodules of MMC, shares the energy supply and water-cooling system with the MMC, and uses the semicontrol device, namely thyristor, to cooperate with the *LC* circuit to realize the control of the energy dissipation function, thus providing a low-cost solution to the FRT problem. Furthermore, the control strategy and parameter matching method are proposed. The 0.75 kV/0.37 MW TCM MMC prototype is built, and the experimental results verify the effectiveness of the proposed scheme. Finally, the performance of TCM MMC in the different FRT process of the ±150 kV/700 MW VSC-HVdc system is analyzed, and the proposed scheme is compared with existing schemes in various aspects.**

***Index Terms*—DC chopper (DCC), fault ride through (FRT), offshore wind VSC-HVdc system, thyristor.**

I. Introduction

In RECENT years, offshore wind power has been developing rapidly due to the characteristics of abundant resources, high power generation utilization hours, no land occupation, and suitability for large-scale development, with a trend of increasing transmission distance and capacity [1], [2]. The voltage source converter (VSC)-HVdc technology based on a modular multilevel converter has become the preferred network mode for large-scale offshore wind power transmission due to its advantages of flexible control and low loss, which has wide application prospects [3].

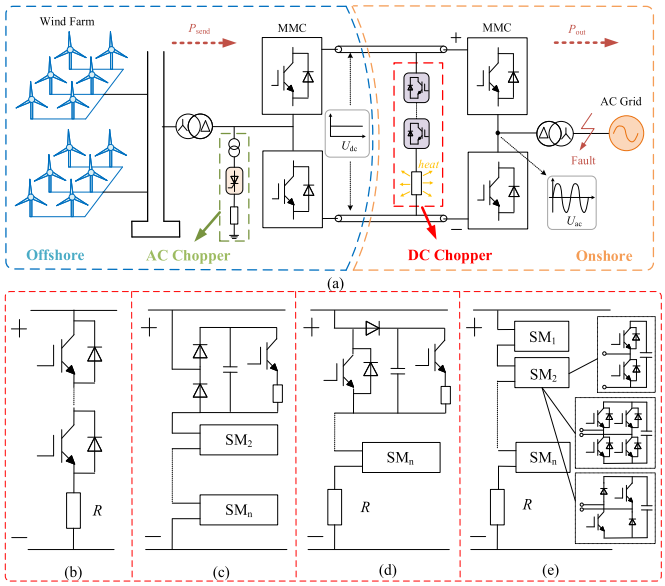

Fig. 1. Offshore wind VSC-HVdc system structure. (a) Offshore wind VSC-HVdc system. (b) Concentrated DCC. (c) Distributed DCC. (d) Hybrid DCC. (e) MMC DCC.

Fig. 1(a) shows the network diagram of the offshore wind VSC-HVdc system. The offshore wind farm collects the electrical energy and transmits it to the sending terminal modular multilevel converter (MMC) via the offshore booster station, and then transmits it to the ac grid through the receiving terminal MMC after dc transmission.

When a fault occurs on the ac side of the receiving terminal MMC, because the power generated by the wind farm remains unchanged for a short time, and the output power of the system decreases, the surplus power in the system will continue to charge the capacitor, resulting in a rapid increase in the dc-link voltage [4]. Taking three-phase short-circuit fault as an example, the dc-link voltage will exceed the allowable peak voltage of the system within 30–50 ms, threatening the safe operation of MMC and other critical equipment, so it is of great significance to realize the fault ride through (FRT) of the offshore wind VSC-HVdc system [5].

Manuscript received 28 February 2023; revised 19 May 2023 and 7 August 2023; accepted 30 September 2023. Date of publication 9 October 2023; date of current version 6 December 2023. This work was supported in part by the National Key Research and Development Program of China under Grant 2021YFB2400602, in part by the National Science Fund for Distinguished Young Scholars of China under Grant 52225701, and in part by the Young Elite Scientists Sponsorship Program by CAST under Grant 2022QNRC001. Recommended for publication by Associate Editor M. ElMoursi. *(Corresponding author: Xiangyu Zhang.)*

The authors are with the State Key Laboratory of Alternate Electrical Power System With Renewable Energy Sources, North China Electric Power University, Beijing 102206, China (e-mail: 120202101019@ncepu.edu.cn; qilei@ncepu.edu.cn; jinmeichen@ncepu.edu.cn; hezhiguo@ncepu.edu.cn; zhangxiangyu@ncepu.edu.cn).

Color versions of one or more figures in this article are available at https://doi.org/10.1109/TPEL.2023.3322986.

Digital Object Identifier 10.1109/TPEL.2023.3322986

The traditional FRT schemes can be divided into two main types: rapidly reducing the power generated by the wind farm and using energy dissipation equipment to absorb surplus power [4], [6]. At present, the method of communication or no communication is mainly used to quickly reduce the power generated by the wind farm. However, the method of communication depends on the reliability of the communication system. The method of no communication, such as the frequency up method and the voltage down method, will cause great electrical stress to the wind turbine or the MMC [7], [8]. In addition, the time for the current method to reduce the power generated by the wind farm to 0 is about 150 ms, whereas the dc-link voltage system will exceed the limit value in 30–50 ms, so the application of this method is limited [9]. The energy dissipation equipment can be divided into ac chopper and dc chopper (DCC). The ac chopper is located at the transformer side of the wind farm outlet, as shown in Fig. 1(a), and consists of thyristors and resistors. The technology is simple, but due to the light requirements of the offshore platform, the mature ac chopper scheme is generally not adopted. Most of the existing projects use the DCC to solve the FRT problem [10], [11].

The DCC is independently placed on the dc side of the land, without the limitation of floor space. The DCC has been applied in more than ten offshore wind power VSC-HVdc projects [12], such as Borwin2 and Helwin1, with broad application prospects, and is mainly divided into four technical routes: concentrated DCC, distributed DCC, hybrid DCC, and MMC DCC.

As shown in Fig. 1(b), the concentrated DCC is composed of a series of fully controlled devices and a concentrated resistor and adopts pulsewidth modulation (PWM) [13]. The concentrated resistor is placed outside and adopts air cooling for heat dissipation. The technology is simple, but there is a problem of voltage unbalance when the series-connected insulated gate-bipolar transistor (IGBT) operates. This problem can be solved by connecting metal-oxide varistors (MOVs) in parallel at both ends of the IGBTs [14]. However, due to the use of two-level modulation, the pulse current has an effect on the dc-link voltage, resulting in a high dc-link voltage ripple of about 10%.

The distributed DCC shown in Fig. 1(c) is composed of many chopper modules [15]. It adopts sine wave modulation and changes the absorbed power by controlling the number of chopper module inputs. Due to the adoption of a smooth control strategy, the ripple of dc-link voltage is relatively small, about 5%. However, the resistor is inactive during normal operation. In the FRT process, the resistor will emit a lot of heat, which affects the operation of power electronic devices. Due to the distribution of the resistors in each module, their heat dissipation design is very strict, requiring expensive water-cooling systems and bringing additional losses.

The hybrid DCC shown in Fig. 1(d) is composed of chopper modules and a concentrated resistor [16]. It realizes the slow change of the current flowing by the concentrated resistor through the gradual input of the chopper modules, thus reducing the impact on the dc-link voltage. Unlike the distributed DCC, the surplus power in the hybrid DCC scheme is mainly absorbed by the resistor placed outside, so the water-cooling system power is smaller.

The MMC DCC, as shown in Fig. 1(e), consists of an MMC submodule (SM) and a concentrated resistor. The MMC SM includes a half-bridge SM, a full-bridge SM, and an asymmetric full-bridge SM [17], [18], [19]. In MMC DCC, the current flowing through the concentrated resistor can be controlled by changing the number of SMs. However, since no resistors are installed in the SMs, a special control strategy is required to make the average current flowing through the SMs 0, thereby achieving voltage balance in the SMs. In this scheme, the MMC module does not require a water-cooling system for heat dissipation, but similar to the hybrid scheme, each SM uses two IGBTs, which is expensive.

From the above analysis, it can be seen that the existing DCCs all use full control devices to realize the turning ON and OFF of dc current, while the full control devices are expensive [10], accounting for more than 40% of the total cost shown in Table IV. The DCC is arranged independently, which requires additional water-cooling system, power supply system, wall bushing, and other equipment. This leads to the high total cost of the existing schemes and limits their further application.

In view of the defects of existing DCCs, this article proposes an MMC with integrated energy dissipation function using thyristor-based chopper modules (TCM MMC), which is described in detail in Section II. The main function of the chopper module is to dissipate the surplus power of the system. Considering the lightweight requirements of offshore converter platforms, the TCM MMC is located in onshore converter stations with lower volume and weight requirements. The TCM MMC distributes the TCMs to the SMs of the onshore MMC. The thyristor is used as the core device to realize the turn-ON of the energy dissipation function, and the thyristor is turned OFF by the *LC* circuit. The TCM shares the water-cooling system with MMC, which has an independent control logic and does not interfere with the normal operation of the MMC.

For the FRT solution using IGBTs [11], it controls the input and output of the chopper module based on the capacitor voltage. When the capacitor voltage is higher than the set value, the IGBT is input, and when the capacitor voltage is lower than the set value, the IGBT is output. In the proposed scheme using the thyristor, it does not have the ability to turn OFF the dc current, so the *LC* circuit is used to help turn it OFF. Due to the fixed oscillation frequency of the *LC* circuit, it adopts a fixed cycle action strategy. During the FRT process, the dc-link voltage is stabilized by gradually turning the thyristors ON and OFF. There are also differences in the voltage and current characteristics of the chopper modules due to the different devices used. In the case of the IGBT, it directly turns OFF the dc current, and due to the effect of stray inductance, there is a voltage overshoot during the turn-OFF process. For the thyristor, it resists the surge current due to the superposition of the oscillating current and the current flowing through the energy dissipation resistor, and there is no voltage overshoot during the turn-OFF process. IGBTs and thyristors also differ in terms of the device manufacturing process and switching losses, resulting in cost and reliability differences between the two schemes. Due to the mature technology of thyristor, if the turn-OFF current capacity limitation is ignored, the cost of using IGBTs when constructing a chopper module

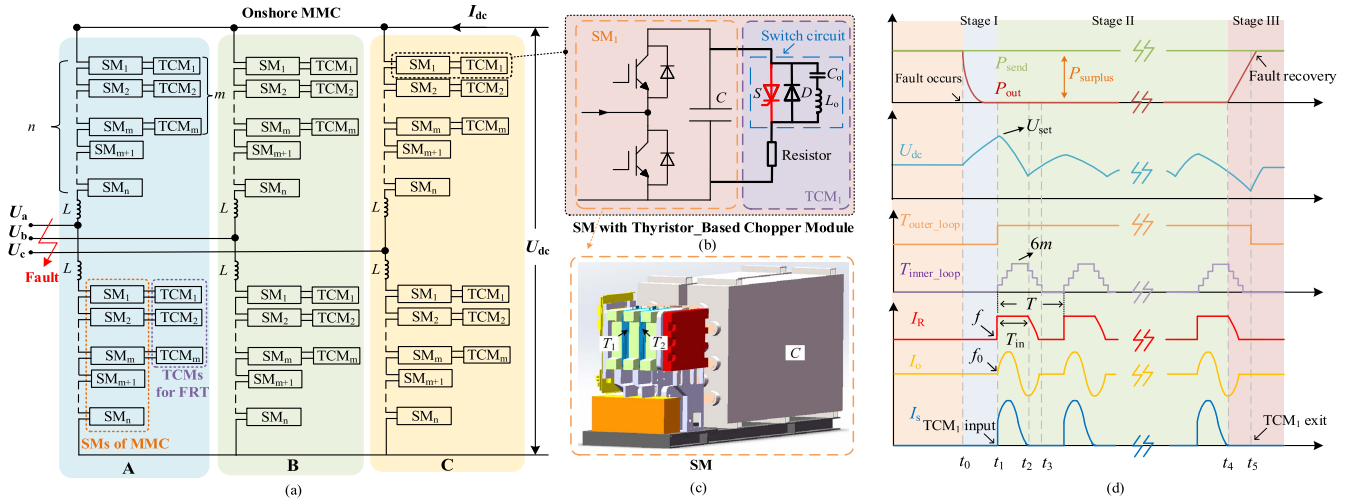

Fig. 2. TCM MMC topology and working principle. (a) TCM MMC. (b) SM with TCM. (c) SM. (d) Working principle.

with the same capacity is about 15%–30% of that of thyristors, and the reliability of thyristors is much higher than that of IGBTs. In addition, compared with IGBT, thyristor has stronger current surge capacity and voltage withstand capacity [20]. Therefore, the scheme proposed in this article greatly reduces the FRT cost of the offshore wind power system, and has high reliability, which has considerable application value.

The rest of this article is organized as follows. Section II introduces the topology and working principle of TCM MMC. In Section III, the TCM MMC parameter selection method is discussed. In Section IV, the prototype equivalent experiment is carried out. Section V analyzes the characteristics of TCM MMC in the FRT process, and Section VI carries out the comparison of different schemes. Finally, Section VII concludes this article.

II. Proposed Novel TCM MMC

A. Topology and Working Principle of TCM MMC

The MMC adopts a modular design, and each half-bridge SM has an independent power supply system and water-cooling system, allowing chopper modules to be distributed in MMC half-bridge SMs. As the thyristor is a semicontrolled device and has no turn-OFF capability, it requires an auxiliary circuit to realize the turn-OFF. Based on the above considerations, the topology proposed in this article is shown in Fig. 2. The TCMs, consisting of switch circuits and energy dissipation resistors, are added to the partial SMs of each bridge arm of the MMC. The switch circuit consists of a thyristor (S), an antiparallel diode (D), an oscillation capacitor (C_o), and an oscillation inductor (L_o).

In normal operation, the thyristor does not operate and the resistor does not dissipate energy. When the fault occurs, the action process of the TCM is shown in Fig. 2(d). First, the thyristor is turned ON, at which point the resistor dissipates energy and the LC circuit also begins to oscillate. When the oscillation current is reversed, the current flowing through the thyristor (I_s) decreases. When I_s is 0, the thyristor is turned OFF, and the current flows through the diode. When the thyristor is turned OFF, the oscillation capacitor is charged until its voltage is equal to that of the SM capacitor, and the energy dissipation process is completed. The detailed operation process of the TCM will be explained in the next part. From the above analysis, it can be seen that the operation of the TCM does not affect the normal operation of the MMC, and because the thyristor is turned OFF at zero current and the loss is low, there is no need for a water-cooling system to dissipate heat during the hundreds of millisecond of the FRT process. In addition, the thyristor can share the energy supply system with the SM, and the energy dissipation resistor can share the water-cooling system with the SM, greatly reducing costs.

Due to the integration of TCM in SM, the reliability of TCM MMC needs to be considered. It is generally believed that the capacitor reliability > the thyristor reliability > the IGBT reliability [20]. Some studies have shown that under MMC operating conditions, the service life of IGBTs is approximately 20–30 years, and the operating life of capacitors is approximately 80–90 years. And in the accelerated aging experiment, the capacitance value of the capacitor changes by only about 5% after 60 000 h [21], [22]. Traditional DCC uses modules consisting of IGBTs and capacitors, whereas the proposed scheme uses modules consisting of thyristors and capacitors. Due to the much lower reliability of IGBTs compared to thyristors, the reliability of the proposed scheme is higher than that of traditional DCC after comprehensive evaluation.

B. Control Logic of TCM MMC

The TCM MMC adopts the dc-link voltage outer-loop control and chopper module input number inner-loop control, as shown in Fig. 3. After a fault occurs, surplus power is gradually dissipated by gradually inputting chopper modules. The chopper modules of six bridge arms act simultaneously to reduce the effect of unbalanced current on MMC operation. When different surplus power needs to be absorbed, due to the fixed surplus power absorbed by each TCM, the number of TCMs that need to be operated is calculated first. Afterward, the six bridge arms

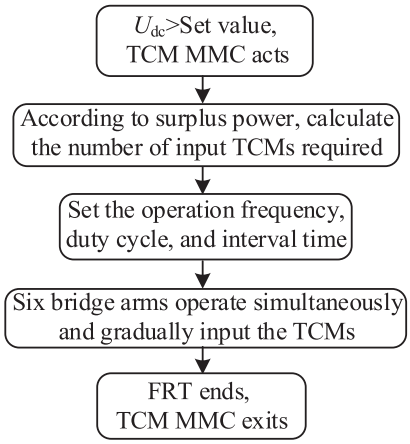

Fig. 3. Control logic of TCM MMC.

gradually input the TCMs according to the parameters given in Section III in the article until the FRT process is completed.

Fig. 2(d) shows the working principle of the TCM MMC during the FRT process. In the figure, P_{send} is the power generated by the wind farm, P_{out} is the power sent from the system, P_{surplus} represents the surplus power, U_{dc} is the system dc-link voltage, $T_{\mathrm{outer\_loop}}$ is the outer-loop control signal, $T_{\mathrm{inner\_loop}}$ is the inner-loop control signal, I_{R} represents the current flowing through the resistor of the TCM, I_{o} is the oscillation current, and I_{s} represents the current flowing through the thyristor. Taking the three-phase short-circuit FRT process as an example, the control logic of the TCM MMC is illustrated as follows.

Stage I (t_0–t_1): Fault Occurrence Stage

Before t_0, the system operates normally, the TCM does not act, and the MMC operates according to the normal control logic. When the fault occurs at t_0, the voltage on the ac side drops rapidly, the system's ability to send power drops, the surplus power charges the capacitor in the system, and the U_{dc} rises. When it reaches the system limit, the TCMs start to operate.

Stage II (t_1–t_4): Surplus Power Dissipation Stage

At t_1, the $T_{\mathrm{outer\_loop}}$ changes from 0 to 1, and the TCM acts in turn. As the thyristor cannot turn OFF the dc current directly like the full control device, it must turn OFF the current through 0 during the reverse period of the oscillating current generated by the *LC* circuit, and the frequency of the oscillating current is fixed, so the input frequency of the TCM is fixed. Taking the TCM_1 of the MMC A-phase upper bridge arm as an example to explain the operation process of the chopper module, when the TCM is put into operation, the thyristor is turned ON, the resistor begins to dissipate surplus power, and the dc-link voltage drops. At the same time, the *LC* circuit begins to generate oscillating current superimposed on the thyristor. The above process is shown in Fig. 4(a). When the oscillating current reverses at t_2, the current flowing through the thyristor gradually decreases to 0, and the thyristor is turned OFF, as shown in Fig. 4(b). It is assumed that each arm has m SMs installed with TCMs. When $P_{\mathrm{surplus}} = P_{\mathrm{rate}}$ (P_{rate} is the rated power

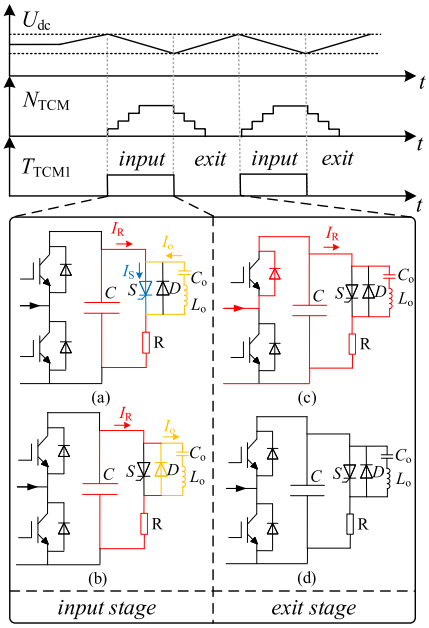

Fig. 4. TCM action process. (a) Thyristor is turned ON. (b) Thyristor is turned OFF. (c) Capacitor charging. (d) TCM exits.

of the system), $6m$ TCMs are used. When $P_{\mathrm{surplus}} = k\mathrm{P}_{\mathrm{rate}}$ ($0 < k < 1$), 6 km TCMs are input. After the thyristor is turned OFF, the chopper module exits at t_2, and U_{dc} gradually rises. At this point, the SM capacitor charges the oscillating capacitor until the voltage of the two is equal, as shown in Fig. 4(c). The surplus power then continues to charge the SM capacitor shown in Fig. 4(d); the TCMs completely exit at t_3 and the dc-link voltage increases. The above process is repeated, and the dc-link voltage is stabilized and fluctuated within a certain range.

Stage III (t_4–t_5): Fault Recovery Stage

At t_4, the ac side voltage begins to recover, and the surplus power gradually decreases. At the moment of the power recovery of the onshore converter station, the power overshoot will occur, causing the U_{dc} to fall below the rated value. The $T_{\mathrm{outer\_loop}}$ then changes to 0, the TCM does not operate, the U_{dc} gradually returns to the rated value, and the system operates normally.

From the above description, it can be observed that each bridge arm consists of a TCM module in parallel with an MMC SM capacitor. The TCM module only operates during FRT periods and discharges the capacitor through an energy dissipation resistor. The control of the SMs and TCM is independent, and they do not affect each other. The thyristor does not need to coordinate with the IGBTs in the MMC SMs. The SMs of the MMC operate according to the strategy of nearest voltage approximation and the TCM operates based on the given stepped waveform during faults. To achieve capacitor voltage balancing, the MMC prioritizes the activation of SMs with the lowest capacitor voltage and deactivates those with the highest voltage during the sorting process. When the TCM operates and reduces the capacitor voltage, the next sorting process of the MMC will activate the SMs with TCMs. Therefore, within the time of FRT

in seconds, all SMs equipped with TCMs will be activated to achieve FRT function.

III. Key Parameter Matching of TCM MMC

For the TCM MMC scheme proposed in this article, m is the number of TCMs configured for each bridge arm. The TCM configuration should follow the principle of minimum cost, provided that the performance requirements are met. The total cost of TCMs is shown in (1), which includes two parts, one is the equipment cost of the TCM (W_{TCM}), and the other is the heat dissipation cost (W_{heat}). The W_{TCM} increases as the increase of the number of TCMs. As the number of TCMs increases, the surplus power that a single TCM needs to absorb decreases, and the W_{heat} decreases

$$W_{\mathrm{all}} = W_{\mathrm{TCM}} + W_{\mathrm{heat}}. \tag{1}$$

The main components of a TCM are the thyristor, capacitor, inductor, and resistor. The total cost of TCM equipment can be expressed as follows:

$$W_{\mathrm{TCM}} = 6m\left(\frac{1}{2}k_1 C_{\mathrm{o}} U_{\mathrm{SM}}^2 + \frac{1}{2}k_2 L_{\mathrm{o}} I_{\mathrm{o}}^2 + k_3 + k_4\right) \tag{2}$$

where k_1 and k_2 are the proportional coefficients of the cost and energy of the capacitor and inductor, respectively, k_3 is the cost of thyristor, and k_4 is the cost of resistor. Due to the close correlation between the cost of capacitors, inductors, resistors, thyristors, and conditions of use, materials, production processes, labor costs, etc., they tend to be biased toward engineering applications, and there is currently no theoretical basis for k_1–k_4. In general, for capacitors and inductors, their cost is considered to be related to energy [4]. For the capacitors and inductors used in the TCM MMC, after consulting with equipment manufacturers and evaluating their usage conditions, k_1 and k_2 are 1.5 and 2 RMB/J, respectively. As for the energy dissipation resistors and thyristors used, in the TCM MMC, the voltage of a single TCM is 2 kV, the current flowing through the energy dissipation resistor is usually between 1 and 2 kA, the energy dissipation of a single TCM is around 2–3 MW, and the FRT time is about 1 s. Based on the above usage conditions and manufacturers' evaluations, the cost of the energy dissipation resistor and thyristor can be considered constant, and k_3 and k_4 are 3000 and 3600 RMB, respectively.

The heat dissipation cost of an individual TCM is related to the average heat dissipation power it has to absorb, so the total heat dissipation cost can be expressed as follows:

$$W_{\mathrm{heat}} = 6mk_5\frac{P_{\mathrm{R}}T_{\mathrm{fault}}}{T_{\mathrm{interval}}} \tag{3}$$

where T_{fault} represents the time of a single FRT process, T_{interval} represents the interval between two FRT processes, and k_5 is the proportional coefficient of heat dissipation cost and average heat dissipation power.

In summary, the total cost of configuring TCMs in MMC can be expressed by (4). It can be seen that W_{all} is closely related to the selected C_{o}, L_{o}, and P_{R}. After taking the minimum W_{all} as a target, the parameters are also mutually constrained by the requirements for dc-link voltage, operating frequency, etc., so the constraint conditions must be considered from the system and TCM levels

$$W_{\mathrm{all}} = 6m\left(\frac{1}{2}k_1 C_{\mathrm{o}} U_{\mathrm{SM}}^2 + \frac{1}{2}k_2 L_{\mathrm{o}} I_{\mathrm{o}}^2 + k_3 + k_4 + k_5\frac{P_{\mathrm{R}}T_{\mathrm{fault}}}{T_{\mathrm{interval}}}\right). \tag{4}$$

A. System Constraints

The TCM configured by MMC must be able to achieve FRT under the most severe three-phase short-circuit fault condition. At this point, the power dissipated by the TCMs should be greater than or equal to the rated power of the system satisfying the following equation:

$$\frac{P_{\mathrm{rate}}}{6} \le mP_{\mathrm{R}} = m\frac{U_{\mathrm{SM}}^2}{R} \tag{5}$$

where U_{SM} represents the capacitor voltage of a single SM.

When the MMC starts to absorb surplus power, the TCM is switched ON and OFF according to the fixed cycle. With the input of the TCMs, the dc-link voltage drops. The dc-link voltage reaches the lower limit ($U_{\mathrm{dc\_min}}$) at the moment before the TCMs exit, which can be represented by (6). For a single TCM, when the input time is T_{in} and the switch period is T, the energy relationship of the system during the FRT can be expressed as (7)

$$U_{\mathrm{dc\_min}} = U_{\mathrm{dc}} - \Lambda u \tag{6}$$

$$6m \cdot P_{\mathrm{R}} \cdot T_{\mathrm{in}} = kP_{\mathrm{rated}} \cdot T \tag{7}$$

where Δu represents the allowable fluctuation range of dc-link voltage.

At the exit stage of the TCM, the power generated by the wind farm charges the equivalent capacitor of the system. It is assumed that the dc-link voltage reaches the upper limit ($U_{\mathrm{dc\_max}}$) before the TCMs are input, which can be expressed by (8). The duration of the exit stage of the TCMs is T_{out}, which is expressed as $T_{\mathrm{out}} = T - T_{\mathrm{in}}$, and the energy relationship of the system can be expressed as (9)

$$U_{\mathrm{dc\_max}} = U_{\mathrm{dc}} + \Lambda u \tag{8}$$

$$kP_{\mathrm{rated}} \cdot (T - T_{\mathrm{in}}) = \frac{1}{2}C_{\mathrm{eq}}\left(U\mathrm{dc\_max}^2 - U\mathrm{dc\_min}^2\right). \tag{9}$$

The operating frequency of the thyristor is calculated to meet the system requirements and the thyristor's own reverse recovery time requirements. According to (6)–(9), the operating frequency f must satisfy (10). Since the operating frequency must be satisfied for any surplus power, and when $kP_{\mathrm{rate}} = 3mP_{\mathrm{R}}$, the frequency reaches its maximum value in (11), the operating frequency of the thyristor must be greater than (11). The duty cycle D can be expressed by (12), which is constant in real operation, generally between 0.4 and 0.6

$$f = \frac{1}{T} = \frac{kP_{\mathrm{rated}}\left(6mP_{\mathrm{R}} - kP_{\mathrm{rated}}\right)}{12mP_{\mathrm{R}}C_{\mathrm{eq}}U_{\mathrm{dc}}\Lambda u} \tag{10}$$

$$f_{\max} = \frac{3mP_{\mathrm{R}}}{4C_{\mathrm{eq}}U_{\mathrm{dc}}\Lambda u} \tag{11}$$

$$0.4 \le D = \frac{T_{\text{in}}}{T} = \frac{kP_{\text{rated}}}{6m \cdot P_{\text{R}}} \le 0.6. \tag{12}$$

During the FRT process, the average capacitor voltage of the SM with TCM decreased from U_{SM} to $U_{\text{SM}} - \Delta u_{\text{SM1}}$, and the average capacitor voltage of the SM without TCM increased from U_{SM} to $U_{\text{SM}} + \Delta u_{\text{SM2}}$

$$U_{\text{dc\_min}} \le m(U_{\text{SM}} - \Delta U_{\text{SM1}}) + (n-m) \times (U_{\text{SM}} + \Delta U_{\text{SM2}}) \le U_{\text{dc\_max}}. \tag{13}$$

B. TCM Constraints

To ensure reliable output of the TCM, the peak reverse current of the *LC* oscillation should be greater than the current flowing through the energy dissipation resistor. In addition, considering the current capacity of the thyristor, the oscillation current should be between 0.5 and 3 kA, which satisfies the following equation:

$$I_{\text{R}} = \frac{U_{\text{SM}}}{R} \le I_{\text{o}} = \sqrt{\frac{C_{\text{o}}}{L_{\text{o}}}} U_{\text{SM}}. \tag{14}$$

To minimize the cost of the capacitor and inductor, the thyristor is turned OFF just at the peak of the reverse current of *LC* oscillation, so the relationship between the oscillation frequency and the operating frequency of the TCM can be expressed by (15), and the oscillation frequency must satisfy (16). In addition, a certain reverse recovery time (t_{rr}) is required after the thyristor is turned OFF, so the exit time must satisfy (17)

$$D\frac{1}{f} = \frac{3}{4}\frac{1}{f_0} \tag{15}$$

$$f_0 = \frac{1}{2\pi\sqrt{L_{\text{o}}C_{\text{o}}}} \tag{16}$$

$$t_{rr} \le T - T_{\text{in}} = \left(1 - \frac{kP_{\text{rated}}}{6m \cdot P_{\text{R}}}\right) T. \tag{17}$$

In summary, taking the lowest total cost expressed in (4) as target and the constraints of the system and TCM in (5)–(17) as the conditions, the values of m, R, L_{o}, and C_{o} can be obtained at the lowest cost. After obtaining the above parameters, the upper and lower limits of the thyristor's operating frequency can be obtained by (11) and (17).

Taking the ±150 kV/700 MW offshore wind VSC-HVdc system as an example, the parameter selection process is explained. The voltage of a single MMC SM is 2 kV, the number of SMs of a single bridge arm is 150, the capacitor of the SM is 9 mF, ignoring the cable capacitor, the equivalent capacitor of the system can be expressed by (18), and the allowable dc-link voltage fluctuation range is generally 5%. The time of a single FRT process is 1 s, and the time interval between two FRTs is 20 min

$$C_{\text{eq}} = \frac{2 \times 6C_{\text{SM}}}{N}. \tag{18}$$

Taking the above parameters into (4)–(18) and the influence of capacitance changes on the oscillation process due to aging of capacitors is also considered in the design of parameters to ensure the reliable turn-OFF of the thyristor, it can be obtained that $m = 45$, $R = 1.5\ \Omega$, $C_{\text{o}} = 1$ mF, $L_{\text{o}} = 1.08$ mH, $f = 80$ Hz after considering a 10% margin.

For thyristors of different powers, suitable thyristors need to be selected according to the system and parameter manual requirements due to their different characteristics such as reverse recovery times. For the 5STP 06D2800 thyristor selected in this article, its reverse recovery time is 400 μs according to the device manual, its operating frequency is 80 Hz, and the TCM exit time is about 6 ms, which ensures that there is enough time for the thyristor to completely turn OFF. Even in the worst-case scenario, where a subsequent fault occurs immediately after the previous fault ends, and it is the most severe three-phase short-circuit fault, the surplus power charges the system capacitors, which typically takes 30–50 ms to rise from the rated value to start the TCM MMC energy dissipation function. During this period, the thyristors have fully recovered and can continue to operate, which ensures the reliable operation of TCM MMC.

In addition, the shared design of the communication and water-cooling systems has been considered. For the communication system, sharing the communication system between the chopper modules and the SM increases the communication demand between the master controller and the TCM controller, which needs to be expanded on the original MMC control system. However, due to the optimization method of configuring chopper modules, only one-third of the SMs in each bridge arm are equipped with chopper modules, resulting in fewer added ports. For the master controller, its computing power can be expanded on the original basis to meet the demand. After evaluation, the added ports in SM driver and increased computing power on the master controller are acceptable.

The design of the water-cooling system is complex and closely related to practical engineering. Due to various factors such as the required heat dissipation power, surrounding environment, and heat dissipation structure design, it is difficult to directly calculate the heat dissipation capacity of the water-cooling system based on parameters such as input and output power and absorbed energy. So, the heat dissipation capacity of the water-cooling system is generally estimated through evaluation. When the chopper module is integrated into the MMC, the original water-cooling system of MMC needs to be expanded accordingly. During the 1–2 s FRT process, the resistor only generates short-term heat. Moreover, the time interval between two faults is more than 20 min. Therefore, the water-cooling system required for the energy dissipation resistor is not designed based on its rated power, but based on the average power. The resistor generates short-term heat during the fault and water-cooling system dissipates heat for a long time after the fault ends, greatly reducing the requirements for the water-cooling system of the original MMC. Due to the scale effect, the cost and volume of the reconstructed MMC water-cooling system, which can take into account the long-term/instantaneous heat dissipation requirements, are much lower than those of the two independent water-cooling systems of MMC and DCC. According to the water-cooling system manufacturer's evaluation, the volume and cost of the integrated water-cooling system are about 0.6 and 0.65 times that of the two independent water-cooling systems, respectively.

Taking a single TCM module as an example, the TCM operates 80 times per second, and the pulse power is 2.6 MW. Fig. 5

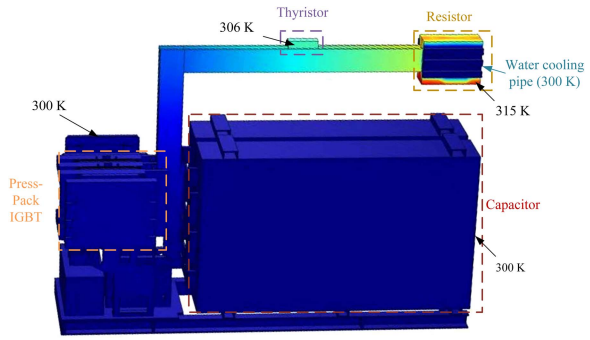

Fig. 5. Impact assessment of chopper module on SM.

TABLE I
EQUIVALENT PARAMETERS OF THE TCM MMC

Item		Values
Auxiliary equipment	Capacitor (C)	16 mF
	Bridge arm inductor (L_s)	0.3 mH
The proposed Chopper Module	Thyristor (S_1)	2.8 kV/0.62 kA
	Diode (D_o)	5 kV/1.03 kA
	Operation frequency (f)	80 Hz
	Energy dissipation resistor (R)	1.5 Ω
	Oscillating capacitor(C_0)	1 mF
	Oscillating inductor(L_0)	1.08 mH

shows an arrangement of the chopper module. In the figure, we assume that the temperature of the water-cooling pipe is constant and the ambient temperature is 300 K. During FRT, the maximum temperature rise of energy dissipation resistor is 15 °C, the maximum temperature rise of thyristor in chopper module is 6 °C, and the temperature of SM is maintained at the initial temperature. Therefore, the chopper module has no impact on the reliability of the normal operation of the SM.

IV. EQUIVALENT EXPERIMENT OF PROTOTYPE

A. Introduction of Prototype

In order to verify the validity of the proposed topology, the TCM MMC equivalent experiment is carried out in this article. The SM equivalent operation test platform is generally used to simulate the normal operation of the MMC SM, as shown in Fig. 6. It consists of four parts: auxiliary power supply, water-cooling system, bridge arm 1, and bridge arm 2. The auxiliary power supply is used to supplement the power loss of the SM action, and the water-cooling system is used to dissipate heat from the SM power electronics [24]. It includes two functions: simulating the normal operation of the MMC SMs and simulating the operation of the chopper modules. During normal operation, the active and reactive power exchanged between the two bridge arms can be given by (19). From this equation, it can be seen that if the modulation ratios M_1 and M_2 are kept constant, the active power exchanged between the two bridge arms can be significantly adjusted by adjusting the phase difference (δ_1–δ_2) of the voltage between the two bridge arms

$$\begin{cases} P = \frac{M_1 M_2 U_{\rm dc}^2}{8X_{\rm L}} \sin(\delta_1 - \delta_2) \\ Q \approx \frac{M_1 U_{\rm dc}^2}{8X_{\rm L}} (M_1 - M_2) \end{cases} \tag{19}$$

where $X_{\rm L} = \omega L_{\rm s}$ is the equivalent impedance between $u_{\rm p1}$ and $u_{\rm p2}$, M_1 and δ_1 are the modulation ratio and phase angle of the bridge arm 1, M_2 and δ_2 are the modulation ratio and phase angle of the bridge arm 2, and P and Q are the active and reactive power exchanged between test bridge arm 1 and test bridge arm 2, respectively.

In the process of simulating FRT process, as indicated by the previous analysis, the result of an ac-side fault in the system is an increase in the voltage of the SM capacitors. For the experimental circuit shown in Fig. 6, the increase in SM voltage can equivalently represent the ac-side fault in the system. Therefore, the auxiliary power supply is temporarily raised in voltage to charge the SM capacitors, thereby simulating the ac-side fault. Once the FRT is completed, the voltage of the auxiliary power supply is lowered to the level of normal operation, thus fully simulating the FRT process.

Since the TCM MMC adopts a modular design and the actions of each module do not affect each other, this article installs the TCM in an SM to verify its function. In order to be equivalent to the real situation, the TCM uses the parameters of the ±150 kV/700 MW offshore wind VSC-HVdc system in Section III. The parameters of the whole experimental platform are given in Table I.

Based on the analysis of experimental equivalency mentioned above, the overall experimental steps are shown in Fig. 7. First, the K is closed and the four SMs are charged to the set voltage through $U_{\rm dc}$. The modulation ratio of both bridge arms is set to 1. The phase angle difference between the bridge arms is gradually increased to simulate the normal operation of the MMC SM. Once the experiment circuit is running stably, adjust the voltage of the auxiliary power supply to increase the voltage to simulate the charging process of surplus power to the SMs. When the voltage reaches the set value, the TCM operates, and the thyristors act according to the set frequency to dissipate energy through the resistors. After five cycles of operation, the TCM stops operating, and the voltage of the auxiliary power supply is adjusted to the rated value, restoring the experimental circuit to normal operation. It should be noted that due to the power limitation of auxiliary power supply, the operation voltage of the SM cannot rise to the 2 kV like that in the actual project, but it does not affect the verification of the function of TCM MMC.

B. Experimental Results

Fig. 8 shows the voltage and current waveform of the TCM. In the figure, $U_{\rm C}$ represents the capacitor voltage of the SM, $I_{\rm arm}$ represents the bridge arm current, $I_{\rm R}$ is the current flowing through the energy dissipation resistor (R), $I_{\rm s}$ is the current flowing through the thyristor, $I_{\rm o}$ is the oscillation current, and $U_{\rm S}$ is the voltage of the thyristor. It can be seen from the figure that before t_0, the SMs operate normally and the capacitor voltage is maintained at around 650 V, with a current of 150 A and a rated

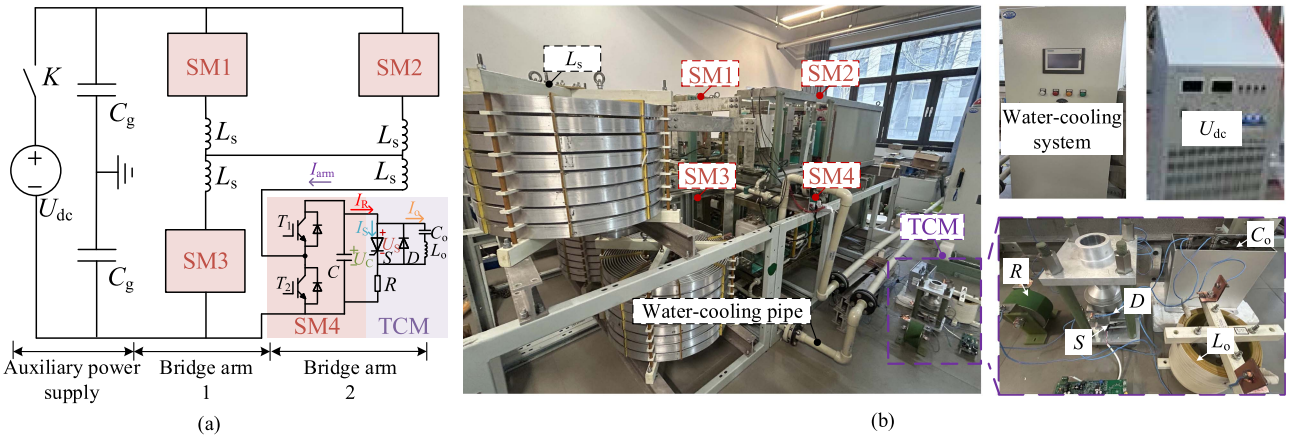

Fig. 6. Experimental principle and site arrangement. (a) Experimental principle. (b) Experimental prototype.

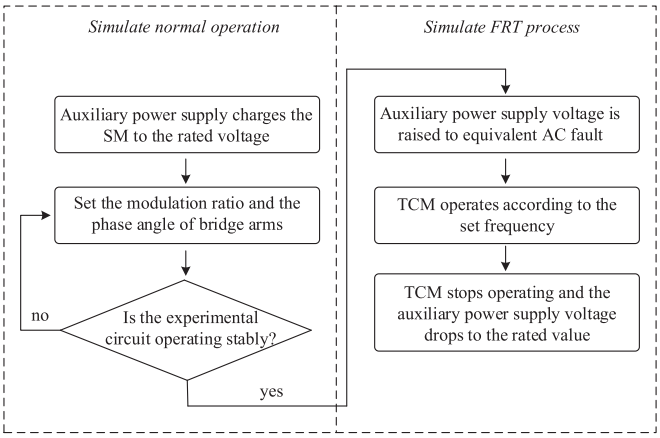

Fig. 7. Steps of the equivalent experiment.

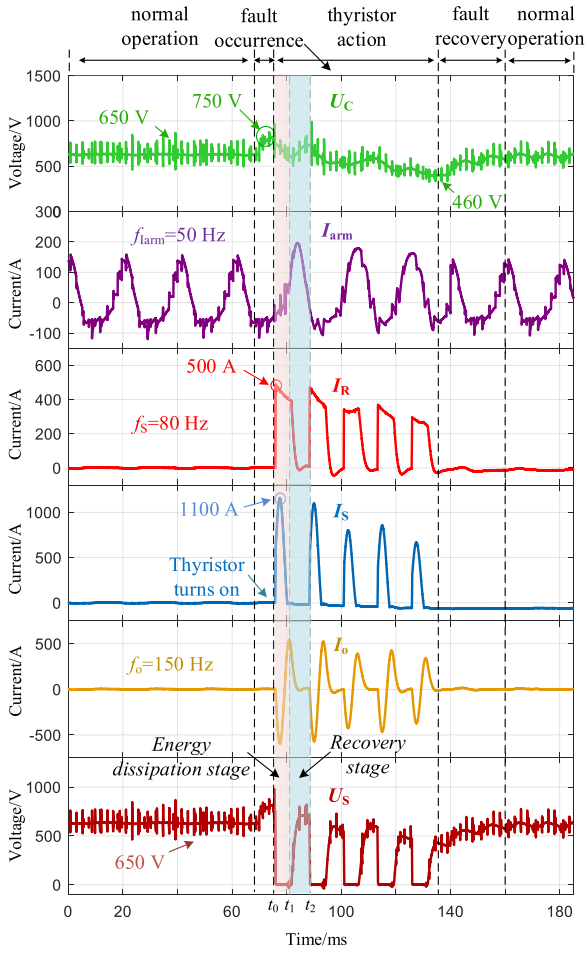

Fig. 8. Experimental results of TCM MMC prototype.

power of 97.5 kW. Due to the switching of the SM, the capacitor voltage has ripple, and the U_S is equal to the U_C.

At t_0, the thyristor operates, and the current flows through the resistor, with a peak value of 500 A. At this time, the U_C begins to decrease, and the energy dissipation power in the single action process is 0.37 MW. It can be seen that with the increase of the oscillation current, the I_s will also increase, up to 1.1 kA. When the oscillation current is reversed, the I_s decreases rapidly, whereas the I_R does not change.

At t_1, the peak value of the reverse oscillation current is reached, and the I_s becomes 0. At this point, the thyristor is turned OFF, the oscillation current continues from the diode in reverse parallel, and the U_S gradually returns to the capacitor voltage of the SM. At this time, the capacitor voltage of SM_4 decreases, whereas the capacitor voltage of other SMs remains unchanged. When the thyristor is closed, the capacitor of other modules charges the SM_4 capacitor and the capacitor voltage of SM_4 increases. After t_2, the process is repeated.

During the energy dissipation stage, the thyristor is turned ON, and the resistor discharges the power from the SM capacitor. During the recovery stage, the bridge arm current charges the SM, causing its voltage to rise. The discharge current is 500 A for a duration of 5 ms, whereas the charging current is 200 A for 7 ms. The capacitance value is 16 mF. The voltage drop during discharge is determined to be 140 V, whereas the voltage rise during charging is approximately 80 V. After five cycles,

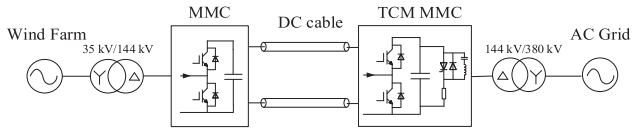

Fig. 9. Simulation model of offshore wind VSC-HVdc system.

the voltage drops from 750 to 460 V. During the experimental process, the voltage drop of the SM is caused by insufficient power from the auxiliary power supply. In practical systems, stable capacitor voltage can be achieved through proper parameter configuration.

From the above analysis, the equivalent experimental results have verified the FRT capability of the TCM, as it can dissipate power as expected and reliably perform multiple operations, demonstrating the feasibility of the proposed scheme.

In addition, during the design process, we have considered the levels of the aforementioned currents and selected thyristors rated at 2.8 kV/0.62 kA and diodes rated at 5 kV/1.03 kA. The purchased capacitor (C_o) and inductor (L_o) also meet the current surge capacity requirements. Furthermore, since the thyristor turns OFF only when the current crosses zero, there is no voltage overshoot due to stray inductance like in fully controlled devices. This makes the system more reliable and eliminates the need for additional protective circuits. However, the full-control device needs to actively control the turn-OFF of dc current, so there is a voltage overshoot due to the effect of stray inductance at the turn-OFF time, its voltage utilization rate is low, and its current surge capacity is also weak, which also further explains the advantages of thyristor as the TCM switch device.

V. TCM MMC Performance Analysis

A. Introduction to Simulation Model

In order to further study the characteristics of TCM MMC in system FRT process, a ±150 kV/700 MW offshore wind VSC-HVdc system is built in power systems computer aided design/electromagnetic transients including DC (PSCAD/EMTDC). The topology of the system is shown in Fig. 9. The voltage of the receiving end ac grid is 380 kV, using the form of an equivalent voltage source. The wind farm outlet voltage is 35 kV, and after boosting, it is connected to MMC, which uses the form of an equivalent current source. The TCM MMC is located at onshore converter station to achieve the FRT capability. The TCM MMC uses the detailed model, and MMC uses the Thevenin equivalent model [23]. The wind farm uses the equivalent power source to speed up the simulation. MMC adopts *V/f* control strategy and TCM MMC adopts V_{dc}/Q control strategy. The most serious three-phase short-circuit fault and most common single-phase short-circuit fault are considered in the simulation process, and the fault duration is 1 s. From the analysis in Section III, the configuration and detailed parameters of the TCMs can be obtained. The system requirements and key parameters in the FRT process are shown in Table II.

TABLE II
System Requirements and the TCM MMC Parameters

Parameter	Value
System rated power (P_{wind})	700 MW
Rated dc-link voltage (U_{dc})	300 kV
Rated dc-link current	2.3 kA
MMC AC side voltage	144 kV
AC Grid voltage	380 kV
DC cable length	90 km
SMs number of single bridge arm (n)	150
SM rated voltage (U_{SM})	2 kV
SM capacitor (C)	9 mF
TCMs number of single bridge arm (m)	45
TCM MMC start condition	$U_{dc} > 1.02$ p.u.
TCM MMC exit condition	$U_{dc} < 0.95$ p.u.
The dc-link voltage peak value	$U_{dc\_max} < 1.1$ p.u.
The dc-link voltage ripple	Less than 5%
SM capacitor voltage fluctuation range	0.6 p.u.$< U_{SM} <$ 1.2 p.u.

B. Analysis of Simulation Results

Fig. 10 shows the waveform of TCM MMC in the three-phase short-circuit FRT process. In the figure, U_{ac} represents the ac voltage at the receiving terminal of the system, Number is the number of the input TCMs, U_{dc} represents the dc-link voltage, U_{SM} represents the SM capacitor voltage with TCM, I_{bridge} represents the phase current of phase A, and $U_{SM\_no\_TCM}$ represents the SM capacitor voltage without TCM. It can be seen from the figure that U_{ac} drops to 0 at $t = 0.1$ s and gradually recovers to the rated value after 1 s. At the beginning of the fault, because the output capacity of the converter station at the receiving terminal is reduced to 0, while the wind farm still sends power to the system, U_{dc} continues to rise. When the set limit is reached, the TCMs of TCM MMC act to absorb the surplus power.

At the initial action stage of the TCMs, because the sequence of the SMs for TCM MMC to put into operation is random, if the SMs are not put into operation with the TCM, although the capacitor voltage of the SM will decrease, it will not lead to the reduction of the dc link voltage. Therefore, it takes some time for the SMs to rotate so that the dc-link voltage drops and stabilizes within the safe range until the fault is over. During the whole FRT period, the peak value of dc-link voltage is 1.09 p.u., and fluctuation range is within 1%, which meets the requirements of the system.

For the TCM, the current flowing through the resistor has the same frequency as the thyristor operating at 80 Hz. The voltage fluctuation range of SM capacitor is between 0.75 and 1.15 p.u., which meets the requirements. For the three-phase short-circuit fault, U_{SM} decreases to 0.75 p.u. after the resistor is consuming energy, whereas $U_{SM\_no\_TCM}$ increases to 1.1 p.u., satisfying the requirement of (13). At the same time, the capacitor voltage of the SM and dc-link voltage also meet the requirements of the system. Since the three-phase short-circuit condition requires TCM MMC to absorb all the power generated by the system, I_{bridge} increases to 1.3 p.u. during the FRT, but since the MMC

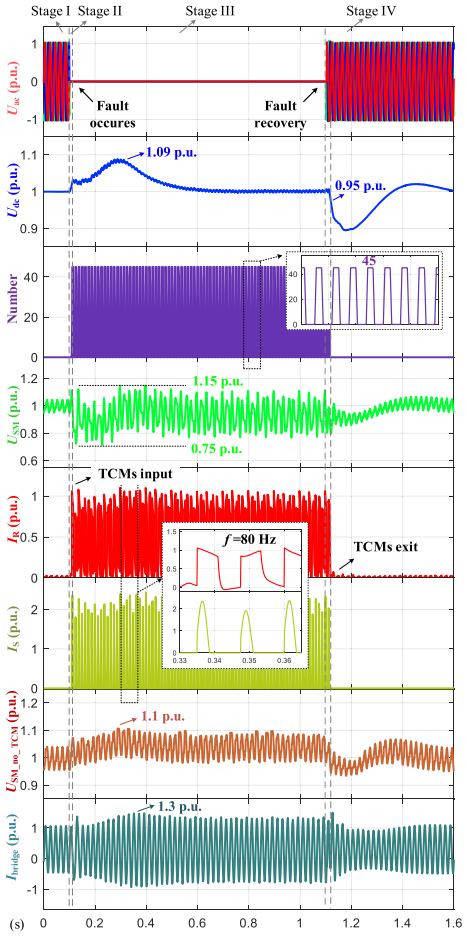

Fig. 10. Simulation results of TCM MMC under three-phase short-circuit FRT process.

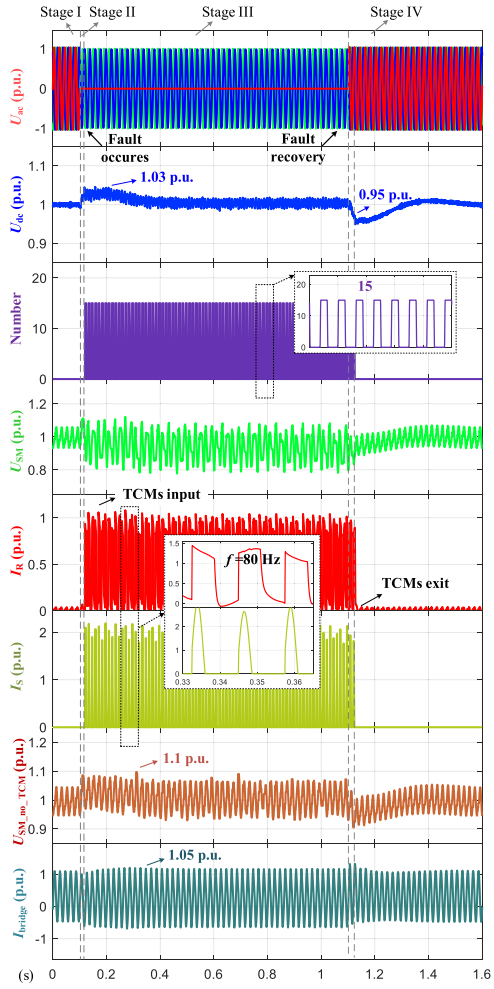

Fig. 11. Simulation results of TCM MMC under single-phase short-circuit FRT process.

is designed with a large margin, the current needs to reach 2 p.u. before the MMC is tripped, so the short-term increase in current is acceptable. When the dc-link voltage drops to 0.95 p.u., the TCMs will exit, and the capacitor voltage will slowly recover to the rated value.

Fig. 11 shows the waveform of the TCM MMC under single-phase short-circuit FRT process. The whole FRT process is basically the same as that of the three-phase short-circuit FRT process. U_{SM} decreases to 0.8 p.u. after the resistor is consuming energy, whereas $U_{\mathrm{SM\_no\_TCM}}$ increases to 1.1 p.u., also satisfying (13). The capacitor voltage of the SM and the dc-link voltage also meet the requirements of the system. However, due to the small number of TCM inputs, the dc-link voltage ripple is larger compared to three-phase short-circuit faults. In addition, compared with the three-phase short-circuit fault, MMC can still transmit power under the single-phase short-circuit fault condition, and the surplus power absorbed by TCM MMC is less, so I_{bridge} only increases to 1.05 p.u. during the FRT, which meets the system requirements.

Further, as shown in the figure, since all SMs are activated simultaneously during a single-phase fault, the surplus power is uniformly absorbed by SMs. This avoids the problem of power imbalance. Fig. 12 shows the upper arm current of different phases of TCM MMC under single-phase short-circuit FRT process, and it can be seen that there is no significant difference between the bridge arm current of different phases, which verifies the effectiveness of the proposed scheme in this article.

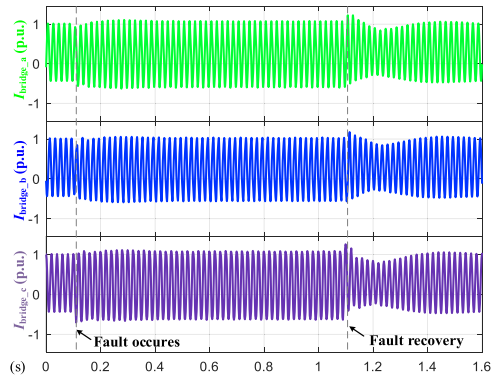

Fig. 12. Upper arm current of different phases of TCM MMC under single-phase short-circuit FRT process.

In addition, Fig. 13 shows the simulation results of the TCM additional losses caused by capacitor voltage fluctuations. From

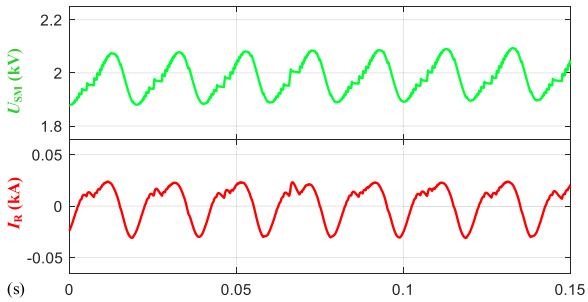

Fig. 13. Simulation results of TCM additional losses.

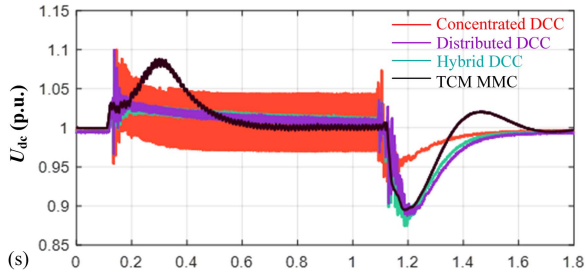

Fig. 14. System DC-link voltage ($U_{\rm dc}$) in various FRT schemes.

the figure, it can be seen that when the MMC operates normally, the ripple of capacitor voltage is about ±5%, and the effective value of $I_{\rm R}$ is about 14 A. Therefore, it can be concluded that the total loss of all chopper modules in the MMC during normal operation is about 0.08 MW, whereas the power loss of the IGBTs in the MMC is about 10 MW [24], and the power loss of chopper modules is about 0.8% of the IGBT power loss, which is acceptable. With the development of technology, more advanced control methods can be adopted to reduce the ripple of the MMC capacitor voltage [25], [26], which will also lead to a reduction in the power loss of chopper modules, and the power loss of TCMs can be further reduced by selecting appropriate *LC* parameters.

To sum up, it can be seen that TCM MMC can maintain the stability of dc-link voltage during the different FRT process without affecting the normal operation of MMC, which further illustrates the effectiveness of the proposed scheme.

VI. Schemes Comparison

In order to illustrate the advantages and disadvantages of the scheme proposed in this article, the performance, cost, volume, and weight of various schemes including concentrated DCC, distributed DCC, hybrid DCC, MMC DCC, and TCM MMC shown in Fig. 1 are compared taking ± 150 kV/700 MW offshore wind VSC-HVdc system as an example.

A. Performance Comparison

Fig. 14 shows the comparison of the system dc-link voltage ($U_{\rm dc}$) in various FRT schemes under three-phase short-circuit conditions. From the figure, it can be seen that for concentrated DCC, due to the adoption of PWM control, the IGBTs turn ON and turn OFF simultaneously, and the pulse current has a greater impact on the system. The dc-link voltage peak value can reach 1.1 p.u., and the dc-link voltage ripple is about 8%. For distributed DCC and hybrid DCC, due to the strategy of gradually putting in and cutting off SMs, the dc-link voltage ripple is lower at about 2% after the dc-link voltage stabilizes. For TCM MMC, the same strategy of gradually putting in and cutting off TCMs is adopted, and due to the larger number of TCMs compared to traditional distributed DCC, the dc-link voltage ripple is lower at about 1%, and the performance of the entire FRT stage meets the system requirements. However, because TCM MMC integrates TCMs with MMC SMs, and the process of putting in and cutting off MMC SMs has a certain randomness, the dc-link voltage will rise to 1.09 p.u. in the initial stage of the fault, which is higher than that of traditional schemes. In summary, different FRT schemes can respond to faults quickly in the initial stage. For independent DCC, since it is installed on the dc bus, it will cause an impact on the dc-link voltage at the moment of operation, resulting in the dc-link voltage peak value appearing in the initial stage of the fault. For the TCM scheme, since it is installed in the MMC, the dc-link voltage peak value will appear after a delay due to the randomness of the SM operation.

A detailed performance analysis is also given in Table III. The TCM MMC only includes chopper modules, the SM in the MMC DCC is a half-bridge module, and a single SM voltage is 2 kV with a total of 150 SMs. The chip area unit (CAU) and the DCC performance that is defined in [15] are used to evaluate the semiconductor usage in various DCC schemes. A single IGBT or thyristor is defined as 1.0 CAU and a single diode is 0.5 CAU. In addition, DCC performance is defined as the DCC power capability per CAU. Higher DCC performance means a higher semiconductor utilization.

The table shows that the concentrated DCC topology is the simplest, uses the least number of IGBTs and diodes, and has the highest DCC performance. However, the IGBTs must operate simultaneously and require a wall bushing, which can cause high ripple in the dc-link voltage. Both distributed DCC and hybrid DCC distribute energy dissipation resistors into each SM, resulting in low dc-link voltage ripple but requiring an independent water-cooling system, which is highly costly. The MMC DCC uses a special control strategy, which eliminates the need for a water-cooling system, but the DCC performance is the lowest. The TCM MMC scheme proposed in this article integrates DCC into MMC, without the need for wall bushings, additional power supply and control systems, and expands on the existing water-cooling system of MMC, resulting in lower heat dissipation costs. In addition, due to the use of thyristors, the cost can be significantly reduced compared to traditional schemes. However, from the table, it can be observed that, under the same capacity, the DCC performance of the proposed scheme (TCM MMC) is lower than that of the concentrated DCC and distributed DCC schemes, and is similar to the Hybrid DCC and MMC DCC schemes. This is because, for independent DCC, each module bears a voltage of 2 kV, requiring a total of 150 modules. In the concentrated DCC scheme, the simplest form of IGBT with energy dissipation resistors in series is used, resulting in the minimum usage number of IGBTs and diodes, thereby

TABLE III
PERFORMANCE ANALYSIS IN VARIOUS SCHEMES

terms	Concentrated DCC	Distributed DCC	Hybrid DCC	MMC DCC	TCM MMC
Required series IGBTs	yes	no	no	no	no
Multilevel capacitor	no	yes	yes	yes	no
Required wall bushing	yes	no	yes	yes	no
Required water-cooling	no	yes	yes	no	yes
min. number of SMs	-	150	150	150	270 (45×6)
Total IGBT/diode/thyristor	150/150/0	150/300/0	300/300/0	300/300/0	0/270/270
Total CAU	225	300.	450	450	405
DCC performance/MW/CAU	3.1	2.3	1.5	1.5	1.7
Control complexity	Require simultaneous action of IGBT	Do not require alternating voltage or current		Require alternating voltage or current	Do not require alternating voltage or current
dc-link voltage ripple	high	low		low	low

TABLE IV
EQUIPMENT AND COST IN DIFFERENT ENERGY DISSIPATION SCHEMES

Equipment	Unit Price	Number				
		Concentrated DCC	Distributed DCC	Hybrid DCC	MMC DCC	TCM MMC
IGBT	8 p.u.	150	150	300	300	0
Diode	0.5 p.u/0.2 p.u.	150	300	300	300	270 (45×6)
Thyristor	1 p.u.	0	0	0	0	270 (45×6)
Support capacitor	2 p.u.	0	150	150	150	0
Oscillating capacitor	1 p.u.	0	0	0	0	270
Oscillating inductor	1 p.u.	0	0	0	0	270
Concentrated Resister	200 p.u.	1	0	1	1	0
Distributed Resistor	1.2 p.u.	0	150	150	0	150
Wall bushing	300 p.u.	1	0	1	1	0
Water-cooling system	300 p.u./30 p.u.	0	Independent	Independent	0	Shared with MMC
Insulating frame, energy supply system, etc	500 p.u./50 p.u.	Independent	Independent	Independent	Independent	Shared with MMC
Total cost		**2275 p.u.**	**2630 p.u.**	**4330 p.u.**	**3850 p.u.**	**1124 p.u.**

achieving the highest DCC performance. On the other hand, in the proposed TCM MMC scheme, according to the parameters in Section III of the manuscript, it is calculated that 45 SMs in each bridge arm require the installation of TCMs. This means that a total of 270 TCMs need to be installed, requiring more thyristors and diodes compared to the traditional scheme. Consequently, the utilization of semiconductor devices is lower, leading to lower DCC performance. Certainly, due to the higher number of TCMs in the proposed scheme compared to the traditional DCC scheme, it can more smoothly absorb surplus power during the FRT process, resulting smaller dc voltage ripple. At the same time, during the FRT process, the capacitance voltage of SMs without chopper modules will increase by about 1.1 times, which is acceptable after evaluation.

B. Cost Comparison

Table IV shows the unit price, number, and total cost of main equipment required by different energy dissipation schemes. It should be noted that the price of power electronic devices in Table IV is obtained from the device suppliers, including IGBT, thyristor, and diode. For other equipment, such as capacitors, inductors, resistors, and water-cooling systems, their prices are closely related to the operation conditions, which are obtained after consulting the corresponding manufacturers for evaluation. For the convenience of comparison, the price of a 2.8 kV/0.6 kA thyristor is 1 p.u. After consulting with the device manufacturer, the price of a 5 kV/1 kA diode is 0.5 p.u., and the price of a 2.8 kV/1.3 kA diode is 0.2 p.u. Table V provides the type, dimension, weight, and other parameters of the equipment used in various schemes, and compares the volume and weight of the MMC half-bridge module, TCM, and distributed DCC SM.

For the 300 kV VSC-HVdc system, the concentrated DCC consists of series IGBTs and the concentrated resistor, as shown in Fig. 1(b). The current that IGBT needs to be turned OFF is 2.3 kA, and there is a voltage overshoot due to the influence of stray inductance when turning OFF, so a large voltage margin needs to be reserved. Therefore, 4.5 kV/3 kA IGBT is selected in the

TABLE V
EQUIPMENT PARAMETERS AND TYPES

Equipment	Device	Type	Dimension (mm)	Weight (kg)	Total volume/weight
Half-bridge SM	IGBT	5SNA 3000K452300	237 × 235 × 32 (L×W×H)	4.3	8×10^8 (mm^3)/ 350 kg
	Capacitor	9 mF	1150 × 180 × 750 (L×W×H)	160	
SM (TCM MMC)	Thyristor	5STP 06D2800	60 × 30 (ϕ × H)	0.3	3×10^7 (mm^3)/ 36 kg
	Diode	5SDD 11T2800	59 × 20 (ϕ × H)	0.2	
	Oscillating capacitor	1 mF	280 × 170 × 240 (L×W×H)	12	
	Oscillating inductor	1.08 mH	240× 260 (ϕ × H)	12	
	Energy dissipation resistor	1.5 Ω	100 × 40 (ϕ × H)	2	
SM (Distributed DCC)	IGBT	5SNA 3000K452300	237 × 235 × 32 (L×W×H)	4.3	3.5×10^7 (mm^3)/ 34 kg
	Diode	5SDD 08T5000	60 × 34 (ϕ × H)	0.2	
	Support capacitor	2 mF	350 × 180 × 300 (L×W×H)	20	
	Energy dissipation resistor	0.8 Ω	80 × 40 (ϕ × H)	1.5	

project. The operating voltage of a single device is 2 kV. A total of 150 IGBTs are required, and the wall bushing is needed to place the concentrated resistor outdoors.

For distributed DCC, it is composed of many chopper modules, which consist of supporting capacitors, IGBT modules, and distributed resistors, as shown in Fig. 1(c). Similarly, 4.5 kV/3 kA IGBT is selected. A single module carries a voltage of 2 kV, and a total of 150 modules are required. Each distributed resistor requires a water-cooling system for heat dissipation.

For hybrid DCC and MMC DCC, there are also 150 modules, and each module uses two 4.5 kV/3 kA IGBTs, two diodes, and a capacitor. The wall bushing is required to arrange the concentrated resistor outdoors.

The scheme proposed in this article is to install 45 TCMs in each bridge arm of MMC. Because the thyristor is turned OFF when the current is 0, there is no voltage spike when it is turned OFF, and it has extremely strong current surge capacity. Therefore, the 2.8 kV/0.62 kA thyristor can be selected.

In addition, it can be seen from Table IV that in the traditional scheme, DCCs are arranged independently, requiring independent insulation frame, energy supply system, etc. Since the chopper module is integrated into the SM of MMC and the cheaper half-control device "thyristor" is used, compared with the distributed DCC arranged independently, although the number of equipment used is increased, the cost of thyristor and *LC* circuit is far lower than the expensive IGBT, and the water-cooling system is expanded on the basis of MMC, the insulation frame is also shared with the original MMC SM. Therefore, after evaluation, the overall cost has been reduced by more than 50%, which has a very high economic efficiency.

C. Volume and Weight Comparison

In Table V, the volume and weight of power electronic devices are obtained by searching the device manual, whereas the volume and weight of capacitors, inductors, and resistors are evaluated by the corresponding equipment manufacturers. The volume and weight of individual modules are estimated after taking into account factors, such as water-cooling system, pressure mounting structure, and insulation framework. The table shows that the volume and weight of the TCM and distributed DCC module are similar, much smaller than the MMC SM. Due to the installation of the TCM in the MMC of the onshore converter station, the weight requirement is relatively low. On this basis, the overall volume, floor area, and weight of the proposed scheme are evaluated.

Due to the limited reports on the detailed dimensions of DCCs in existing research, and the detailed dimensions of TCM MMC also need to be obtained after engineering design. Therefore, this article only provides a rough quantitative comparison of the size of the distributed DCC and the TCM MMC based on the completed projects for reference.

The distributed DCC consists of 150 SMs and requires a large independent water-cooling system, which is placed indoors in the form of energy dissipation valves. Based on the completed project, the estimated 300 kV energy dissipation valve requires an area of approximately 50 m^2 and a height of over 10 m.

The TCM MMC requires the installation of a TCM on the MMC half-bridge SM, with 45 additional modules per bridge arm, totaling 270. From Table V, it can be seen that the volume of a single TCM is approximately 1/16 of the volume of the MMC SM. The area of 300 kV MMC is 90 m^2 and the height is 10 m [27]. Due to the consideration of insulation and heat dissipation issues during the design of MMC, there is a large internal space, and factors such as expansion of the water-cooling system are considered. After comprehensive evaluation, TCM MMC is expected to increase its area and volume by 25% on the basis of the original converter valve, which means that the area of TCM MMC is 112 m^2. The total area of the independent DCC + MMC is 140 m^2. In summary, compared to the traditional scheme, the TCM MMC can reduce the total area and volume by approximately 20%.

Since the weight cost is closely related to parameters such as engineering layout, ground bearing capacity, MMC structural

design, etc., it is difficult to provide quantitative comparison. Therefore, this article only qualitatively evaluated the weight costs. From Table V, it can be seen that the weight of a single TCM is similar to that of a single distributed DCC SM, both being about 10% of a single MMC SM. The number of TCMs in the TCM MMC is 270, whereas the number of distributed DCC SMs is 150, making the number of TCMs about 1.8 times that of distributed DCC SMs, and the weight of the module is also 1.8 times that of distributed DCC SMs. However, as the TCMs are integrated into the MMC and are only installed in one-third SMs of each bridge arm, the MMC design retains a considerable margin, and the ground bearing capacity in the onshore converter station is specially designed. After comprehensive evaluation, the weight cost increase of the TCM MMC is basically the same as that of the independent DCC.

After the above comparison, it can be seen that regardless of whether it is for independent DCC or the suggested concept, both aim to achieve stable dc-link voltage during FRT and utilize resistors for dissipating surplus power at the lower-level logic. The difference lies in the fact that for independent DCC, it is separately installed between the dc buses and achieves surplus power dissipation by adjusting the current flowing through the energy dissipation resistors. On the other hand, the proposed TCM MMC scheme integrates the TCM with the SMs of the MMC itself. It controls the current flowing through the resistors dispersed in the MMC bridge arms to equivalent to dissipate surplus power.

For independent DCC, since it is separately installed, it only functions during FRT and does not operate during normal system operation. It operates independently during faults, ensuring that it does not affect the operation of the MMC. However, due to its separate installation, independent DCC requires independent systems for water-cooling, control protection, and power supply, which can result in additional costs.

For the proposed TCM MMC scheme, integrating the TCM into the SMs of the MMC allows for the shared use of water-cooling, control protection, and power supply systems to a certain extent, resulting in significant cost savings and lower dc-link voltage ripple. However, since the TCM is connected in parallel to the capacitors of the SMs and dissipates surplus power by discharging the SM capacitors, it can have an impact on the voltage and current of the MMC itself during FRT. The specific analysis can be found in Section V and will not be repeated again.

VII. Conclusion

In view of the defects that the existing DCCs use a large number of fully controlled devices, which are arranged independently and have a high cost, this article proposes a TCM MMC topology, which disperses the chopper modules into the SMs of the MMC. The TCMs share the water-cooling system, energy supply system, and other systems with the SMs, and replace the expensive fully controlled devices through the coordination of the thyristor and the *LC* circuit, realizing the control of the TCMs, which provides an economic and effective solution for the FRT problem. TCM MMC adopts the dc-link voltage outer loop control and the TCM input number inner loop control strategy to ensure that the dc-link voltage meets the system requirements during the fault.

In this article, TCMs configuration strategy and key parameter selection method are proposed, and a design example of $\pm$150 kV/700 MW offshore wind VSC-HVdc system is given. The 0.75 kV/0.37 MW TCM MMC prototype is built, and the experimental results show the feasibility of the TCM MMC scheme. Further, the system simulation is carried out and the characteristics of TCM MMC in system FRT process are analyzed. The simulation results verify the FRT capability of the TCM MMC. Finally, the proposed scheme and the existing DCCs are compared from different aspects. Compared to traditional solutions, TCM MMC has significant advantages in reducing costs and floor space by 50% and 20%, respectively.

References

[1] M. de Prada, L. Igualada, C. Corchero, O. Gomis-Bellmunt, and A. Sumper, "Hybrid AC-DC offshore wind power plant topology: Optimal design," *IEEE Trans. Power Syst.*, vol. 30, no. 4, pp. 1868–1876, Jul. 2015.

[2] G. Abeynayake, T. Van Acker, D. V. Hertem, and J. Liang, "Analytical model for availability assessment of large-scale offshore wind farms including their collector system," *IEEE Trans. Sustain. Energy*, vol. 12, no. 4, pp. 1974–1983, Oct. 2021.

[3] L. Zeni et al., "Power oscillation damping from VSC–HVDC connected offshore wind power plants," *IEEE Trans. Power Del.*, vol. 31, no. 2, pp. 829–838, Apr. 2016.

[4] A. M. Rauf, V. Khadkikar, and M. S. El Moursi, "A new fault ride-through (FRT) topology for induction generator based wind energy conversion systems," *IEEE Trans. Power Del.*, vol. 34, no. 3, pp. 1129–1137, Jun. 2019.

[5] W. Li, M. Zhu, P. Chao, X. Liang, and D. Xu, "Enhanced FRT and postfault recovery control for MMC-HVDC connected offshore wind farms," *IEEE Trans. Power Syst.*, vol. 35, no. 2, pp. 1606–1617, Mar. 2020.

[6] S. B. Naderi, M. Negnevitsky, and K. M. Muttaqi, "A modified DC chopper for limiting the fault current and controlling the DC-link voltage to enhance fault ride-through capability of doubly-fed induction-generator-based wind turbine," *IEEE Trans. Ind. Appl.*, vol. 55, no. 2, pp. 2021–2032, Mar./Apr. 2019.

[7] G. Ramtharan, A. Arulampalam, and J. B. Ekanayake, "Fault ride through of fully rated converter wind turbines with AC and DC transmission systems," *IET Renewable Power Gener.*, vol. 3, no. 4, pp. 426–438, Dec. 2009.

[8] L. Xu, L. Yao, and C. Sasse, "Grid integration of large DFIG-based wind farms using VSC transmission," *IEEE Trans. Power Syst.*, vol. 22, no. 3, pp. 976–984, Aug. 2007.

[9] M. Ndreko, A. Bucurenciu, M. Popov, and M. A. M. M. van der Meijden, "On grid code compliance of offshore MTDC grids: Modeling and analysis," in *Proc. IEEE Eindhoven PowerTech*, Eindhoven, The Netherlands, 2015, pp. 1–6.

[10] L. Qi et al., "A low-cost DC chopper with coupling transformer for offshore wind VSC-HVdc system," *IEEE Trans. Power Electron.*, vol. 37, no. 5, pp. 4979–4984, May 2022.

[11] S. Wu et al., "A modular multilevel converter with integrated energy dissipation equipment for offshore wind VSC-HVDC system," *IEEE Trans. Sustain. Energy*, vol. 13, no. 1, pp. 353–362, Jan. 2022.

[12] V. Hussennether et al., "Projects BorWin2 and HelWin1—Large scale multilevel voltage-sourced converter technology for bundling of offshore windpower," in *Proc. CIGRE B4-306*, pp. 4–5, 2012.

[13] J. Maneiro, S. Tennakoon, C. Barker, and F. Hassan, "Energy diverting converter topologies for HVdc transmission systems," in *Proc. 15th Eur. Conf. Power Electron. Appl.*, 2013, pp. 1–10.

[14] C. Xu, X. Zhang, Z. Yu, B. Zhao, Z. Chen, and R. Zeng, "A novel DC chopper with MOV-based modular solid-state switch and concentrated dissipation resistor for $\pm$400 kV/1100 MW offshore wind VSC-HVDC system," *IEEE Trans. Power Electron.*, vol. 35, no. 5, pp. 4483–4488, May 2020.

[15] A. Birkel, A. Schön, and M. Bakran, "Analysis and semiconductor-based comparison of energy diverting converter topologies for HVDC transmission systems," in *Proc. 17th Eur. Conf. Power Electron. Appl.*, Geneva, Switzerland, 2015, pp. 1–10.

[16] B. Xu, C. Gao, J. Zhang, J. Yang, B. Xia, and Z. He, "A novel DC chopper topology for VSC-based offshore wind farm connection," *IEEE Trans. Power Electron.*, vol. 36, no. 3, pp. 3017–3027, Mar. 2021.
[17] M. Ramet, J. Outram, L. Cheng, and R. Mukhedkar, "Application of dynamic braking systems in off-shore connected VSC HVdc," in *Proc. 13th IET Int. Conf. AC DC Power Transmiss.*, 2017, pp. 1–4.
[18] S. Cao et al., "Energy dissipation of MMC-HVdc based onshore wind power integration system with FB-DBS and DCCB," *IET Renewable Power Gener.*, vol. 14, pp. 222–230, 2020.
[19] Z. Li et al., "Energy diverting converter topology using unidirectional current H-bridge submodules for VSC-HVDC transmission system," *IEEE Trans. Power Electron.*, vol. 37, no. 5, pp. 5299–5308, May 2022.
[20] F. Naseri and H. Samet, "A comparison study of high power IGBT-based and thyristor-based AC to DC converters in medium power DC arc furnace plants," in *Proc. 9th Int. Conf. Compat. Power Electron.*, Costa da Caparica, Portugal, 2015, pp. 14–19.
[21] W. Zhang et al., "In situ diagnosis of multichip IGBT module wire bonding faults based on collector voltage undershoot," *IEEE Trans. Ind. Electron.*, vol. 70, no. 3, pp. 3045–3054, Mar. 2023.
[22] H. Soliman, H. Wang, and F. Blaabjerg, "A review of the condition monitoring of capacitors in power electronic converters," *IEEE Trans. Ind. Appl.*, vol. 52, no. 6, pp. 4976–4989, Nov./Dec. 2016.
[23] R. Zeng et al., "Integrated gate commutated thyristor-based modular multilevel converters: A promising solution for high-voltage DC applications," *IEEE Ind. Electron. Mag.*, vol. 13, no. 2, pp. 4–16, Jun. 2019.
[24] B. Zhao et al., "Practical analytical model and comprehensive comparison of power loss performance for various MMCs based on IGCT in HVDC application," *IEEE J. Emerg. Sel. Topics Power Electron.*, vol. 7, no. 2, pp. 1071–1083, Jun. 2019.
[25] M. Huang, Z. Kang, W. Li, J. Zou, X. Ma, and J. Li, "Modified modular multilevel converter with third-order harmonic voltage injection to reduce submodule capacitor voltage ripples," *IEEE Trans. Power Electron.*, vol. 36, no. 6, pp. 7074–7086, Jun. 2021.
[26] B. Li, Y. Zhang, G. Wang, W. Sun, D. Xu, and W. Wang, "A modified modular multilevel converter with reduced capacitor voltage fluctuation," *IEEE Trans. Ind. Electron.*, vol. 62, no. 10, pp. 6108–6119, Oct. 2015.
[27] Q. Song et al., "A modular multilevel converter integrated with DC circuit breaker," *IEEE Trans. Power Del.*, vol. 33, no. 5, pp. 2502–2512, Oct. 2018.

Sihang Wu was born in Huangshan, Anhui, China, in 1997. He received the B.S. degree in electrical engineering in 2019 from North China Electric Power University, Beijing, China, where he is currently working toward the Ph.D. degree in electrical engineering.

His current research focuses on fault ride through scheme of offshore wind VSC-HVdc system.

Lei Qi was born in Nanyang, Henan, China, in 1978. He received the B.S., M.S., and Ph.D. degrees in electrical engineering from North China Electric Power University, Baoding, China, in 2000, 2003, and 2006, respectively.

He is currently a Professor of electrical engineering with North China Electric Power University. His research interests include electromagnetic fields theory and application, electromagnetic compatibility in power systems, and advanced power transmission technology.

Meichen Jin was born in Harbin, Heilongjiang Province, China, in 1999. She received the B.S. degree in electrical engineering from North China Electric Power University, Baoding, China, in 2021. She is currently working toward the master's degree in electrical engineering with North China Electric Power University, Beijing, China.

She is currently working on flexible dc transmission.

Zhiguo He was born in Dezhou, Shandong, China, in 1998. He received the B.S. degree in electrical engineering from Shandong University of Technology, Zibo, China, in 2020. He is currently working toward the M.S. degree in electrical engineering with North China Electric Power University, Beijing, China.

His current research focuses on equivalent test of converter valve.

Xiangyu Zhang received the B.S. and Ph.D. degrees in electrical engineering from the Department of Electrical Engineering, Tsinghua University, Beijing, China, in 2015 and 2020, respectively.

He is currently an Associate Professor of electrical engineering with North China Electric Power University, Beijing, China. His research interests include power semiconductor devices, dc circuit breakers, and high-voltage dc systems.